IFN- Hinders Recovery from Mucosal Inflammation during Antibiotic Therapy for Salmonella Gut Infection

Dolowschiak, Tamas ; Mueller, Anna Angelika ; Pisan, Lynn Joanna ; Feigelman, Rounak ; Felmy, Boas ; Sellin, Mikael Erik ; Namineni, Sukumar ; Nguyen, Bidong Dinh ; Wotzka, Sandra Yvonne ; Heikenwalder, Mathias ; von Mering, Christian ; Mueller, Christoph ; Hardt, Wolf-Dietrich

DOI: https://doi.org/10.1016/j.chom.2016.06.008

Article

Cell Host & Microbe

IFN-γ Hinders Recovery from Mucosal Inflammation during Antibiotic Therapy for *Salmonella* Gut Infection

Graphical Abstract

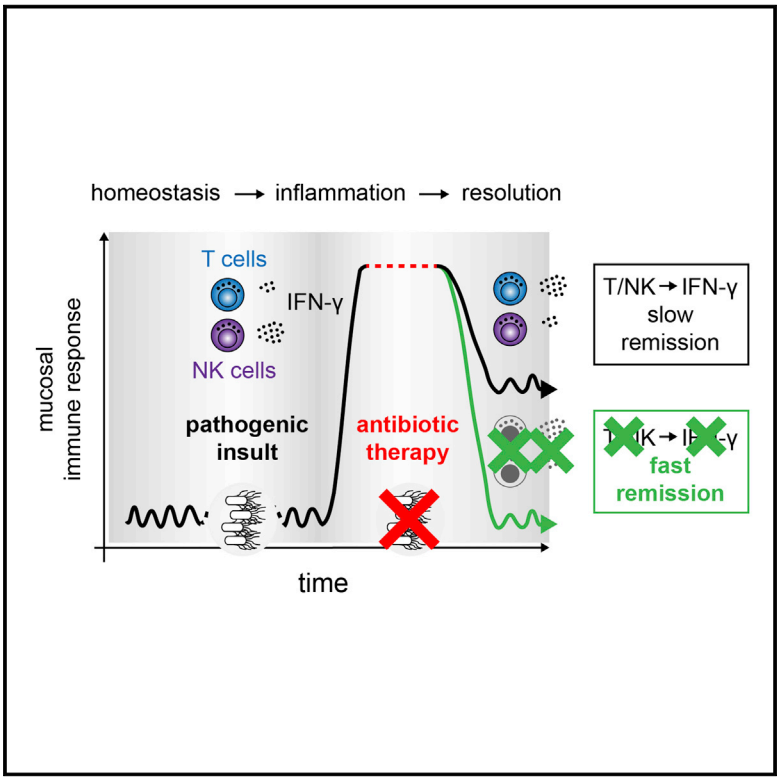

Authors

Tamas Dolowschiak, Anna Angelika Mueller, Lynn Joanna Pisan, ..., Christian von Mering, Christoph Mueller, Wolf-Dietrich Hardt

Correspondence

dtamas@ethz.ch (T.D.), hardt@micro.biol.ethz.ch (W.-D.H.)

In Brief

For unknown reasons, antibiotics are ineffective for curing acute *Salmonella* diarrhea. Dolowschiak et al. find that disease pathology is prolonged by an IFN-γ response of mucosal T and NK cells. Targeting this axis may facilitate the design of effective therapies.

Highlights

- Acute *Salmonella* infection elicits IFN-γ responses that remain during antibiotic therapy
- IFN-γ sustains STAT1 and cytokines, while blocking IL-22/REGIII defenses
- T- and NK cell-derived IFN-γ delays the resolution of mucosal pathology
- IFN-γ could be targeted for accelerating resolution

Dolowschiak et al., 2016, Cell Host & Microbe *20*, 238–249
August 10, 2016
http://dx.doi.org/10.1016/j.chom.2016.06.008

CellPress

CellPress

Cell Host & Microbe
Article

IFN-γ Hinders Recovery from Mucosal Inflammation during Antibiotic Therapy for *Salmonella* Gut Infection

Tamas Dolowschiak,[1,*] Anna Angelika Mueller,[1] Lynn Joanna Pisan,[1] Rounak Feigelman,[2,3] Boas Felmy,[1] Mikael Erik Sellin,[1] Sukumar Namineni,[4] Bidong Dinh Nguyen,[1] Sandra Yvonne Wotzka,[1] Mathias Heikenwalder,[4,5] Christian von Mering,[2,3] Christoph Mueller,[6] and Wolf-Dietrich Hardt[1,*]

[1]Institute of Microbiology, ETH Zurich, 8093 Zurich, Switzerland
[2]Department of Molecular Life Sciences, University of Zurich, 8057 Zurich, Switzerland
[3]Swiss Institute of Bioinformatics, 1015 Lausanne, Switzerland
[4]Institute of Virology, TU Munich, 81675 Munich, Germany
[5]Division of Chronic Inflammation and Cancer, DKFZ, 69121 Heidelberg, Germany
[6]Institute of Pathology, University of Bern, 3010 Bern, Switzerland
*Correspondence: dtamas@ethz.ch (T.D.), hardt@micro.biol.ethz.ch (W.-D.H.)
http://dx.doi.org/10.1016/j.chom.2016.06.008

SUMMARY

Salmonella Typhimurium (_S_.Tm) causes acute enteropathy resolving after 4–7 days. Strikingly, antibiotic therapy does not accelerate disease resolution. We screened for factors blocking remission using a _S_.Tm enterocolitis model. The antibiotic ciprofloxacin clears pathogen stool loads within 3–24 hr, while gut pathology resolves more slowly (ψ_{50}: ~48 hr, remission: 6–9 days). This delayed resolution is mediated by an interferon-γ (IFN-γ)-dependent response that is triggered during acute infection and continues throughout therapy. Specifically, IFN-γ production by mucosal T and NK cells retards disease resolution by maintaining signaling through the transcriptional regulator STAT1 and boosting expression of inflammatory mediators like IL-1β, TNF, and iNOS. Additionally, sustained IFN-γ fosters phagocyte accumulation and hampers antimicrobial defense mediated by IL-22 and the lectin REGIIIβ. These findings reveal a role for IFN-γ in delaying resolution of intestinal inflammation and may inform therapies for acute _Salmonella_ enteropathy, chronic inflammatory bowel diseases, or disease resolution during antibiotic treatment.

INTRODUCTION

Non-typhoidal salmonellosis (NTS) is among the main causes of bacterial diarrhea worldwide (Kirk et al., 2015). Infection with NTS strains like *S*. Typhimurium (*S*.Tm) typically causes acute, self-limiting inflammatory gastroenteritis in man. Infants aged <3 months, the elderly aged ≥60 years and immunocompromised individuals are at risk of systemic pathogen spread that warrants antimicrobial therapy (Onwuezobe et al., 2012). Ciprofloxacin, a third-generation 5-fluoroquinolone is commonly used against both Gram positives and negatives, including systemic NTS infections (Sirinavin and Garner, 2000). Despite its merits in containing systemic infection and ablating fecal shedding, the antibiotic therapy of NTS diarrhea is surprisingly ineffective in reducing the disease symptoms of acute gastroenteritis (Onwuezobe et al., 2012). The mechanistic underpinnings have remained obscure.

The gut mucosa provides an effective barrier against the outer world of microbial habitats. Maintenance of mucosal homeostasis relies on a delicate network of interactions between the microbiota, the stromal compartments, and the gut-associated immune system (Germain, 2012). From birth on, this system evolves in response to the encountered microbes toward an equilibrium that establishes a physiological and immunological superorganism defined by the coexistence of host and its microbes (Eberl, 2010). In the case of acute infections, which often involve pronounced mucosal perturbations, recovery not only requires pathogen elimination, but also relies on mechanisms to resolve inflammation. It has often been assumed that pathogen clearance and the resolution of inflammation should go hand in hand, as resolution kinetics are controlled by the removal of microbe-derived stimuli (Buckley et al., 2013); otherwise, chronic inflammation, or even mortality, may result due to an uncontrolled cytokine storm (Gros and Belkaid, 2014). Indeed, studies of self-limiting acute inflammatory responses led to the discovery of specialized pro-resolving mediators, whose role during the resolution of inflammation has been well established (Chiang et al., 2012; Serhan, 2014). In spite of this progress, the mechanisms controlling remission in the intestinal mucosa have not been fully understood. This includes the failure of antibiotics to relieve enteropathy inflicted by acute NTS diarrhea (Onwuezobe et al., 2012).

Here, we used a murine *Salmonella* diarrhea model (Kaiser et al., 2012) to study the factors limiting resolution during ciprofloxacin therapy. We analyzed resolution kinetics using morphological, cellular, and molecular parameters. Our results delineate how mucosal remission proceeds following pathogen clearance and identified an unresolved interferon (IFN)-γ-driven pro-inflammatory program that hinders mucosal recovery from acute gut infection.

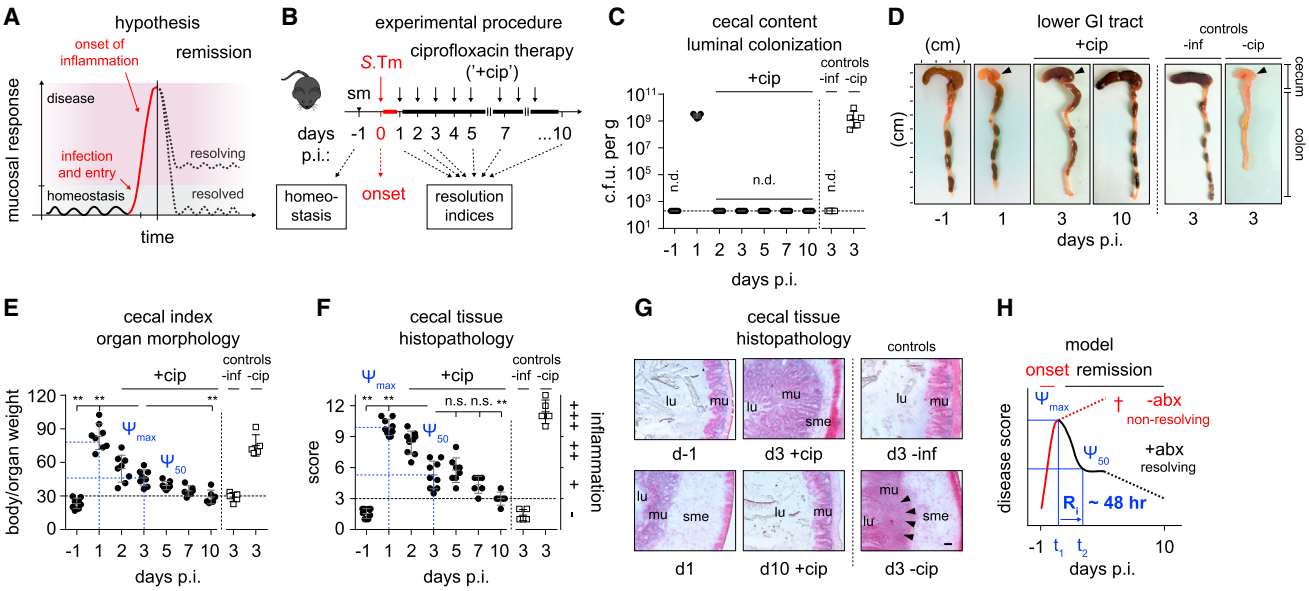

Figure 1. Resolution Kinetics of Mucosal Inflammation during Antibiotic Therapy of Acute *S.* Typhimurium Infection

(A) Schematic illustrating remission scenarios.

(B) Experimental procedure: Bl6 mice were orally infected with 5 × 10^7 CFU *S.*Tm and treated with ciprofloxacin per os from day 1 p.i.

(C) *S.*Tm load in cecal content.

(D) Cecal/colonic macropathology.

(E) Cecal index determined as body weight/excised cecal organ weight.

(F) Histopathology scoring of cecal tissue.

(G) H&E-stained cecal tissue sections. Scale bar, 100 μm.

(H) Remission kinetics of murine *S.*Tm colitis. Summary graphs show n = 5–9 mice from two to five independent experiments as mean ± SD. Statistical significance was calculated via the Mann-Whitney U test. −1, mice w/o sm; p.i., post-infection; n.d., not detectable; +cip, oral ciprofloxacin treatment; -inf, only treatment, no infection; -cip, only infection, no treatment; Ψ_{max}, inflammation at day 1 p.i.; Ψ_{50}, 50% of Ψ_{max}; lu, lumen; mu, mucosa; sme, submucosal edema; †, death.

RESULTS

A Mucosal Remission Model for NTS Enteritis

In the streptomycin mouse model (Kaiser et al., 2012), Bl6 mice infected with *S.*Tm SL1344 develop enteropathy ~12 hr post infection (p.i.). If left untreated, the animals succumb to infection at approximately day 5 p.i. Here, we asked whether antibiotic therapy would not only reduce pathogen loads, but also attenuate pathology and result in resolution of acute mucosal inflammation (Figure 1A). Mice were infected with wild-type (WT) *S.*Tm (5 × 10^7 colony-forming unit [CFU] by gavage) and treated with ciprofloxacin from day 1 p.i. up to day 10 p.i. (Figure 1B, (Kaiser et al., 2014)). Antibiotic therapy reduces gut luminal *S.*Tm loads by 10^7-fold within ~3 hr and prevents pathogen spread to the spleen (Kaiser et al., 2014). Importantly, gut luminal pathogen loads remained below detection, as long as the antibiotic treatment was continued (Figure 1C).

Next, we assessed the resolution of mucosal pathology. In acute self-limiting peritonitis, the resolution interval (R_i) defines the transition time from maximal (Ψ_{max}) to half-maximal inflammation (Ψ_{50}) (Chiang et al., 2012). In analogy, we assessed macroscopic organ morphology and histopathological scoring of the infected cecal tissue at day 1 p.i. to define Ψ_{max}. The macroscopic shrinking of the cecum tissue (Figures 1D and 1E) and the microscopic assessment of tissue histopathology (Figures 1F and 1G) yielded equivalent resolution kinetics reaching Ψ_{50} within ~48 hr and resolution to normal levels within 6–9 days of therapy (Figure 1H). However, it remains to be established which cellular and molecular parameters impact on remission under these conditions.

Transcriptional Response of the Resolving Cecal Mucosa during Therapy

To begin our mechanistic analysis of remission, we performed transcriptional profiling of the cecal tissue. Gene expression of 52 inflammatory cytokines, chemokines, and antimicrobial effectors was quantified using a real-time qPCR array (four mice per group; Table S1). Some of these candidates were known to be induced during acute *S.*Tm infection (Godinez et al., 2008). Our quantitative approach verified the robust expression of many pro-inflammatory genes at Ψ_{max} (Figure 2A, dark blue) and identified their remission kinetics during antibiotic therapy. Hierarchical clustering identified five gene clusters (0.95 p value threshold via multiscale bootstrap resampling; Figures 2B, S1A, and S1B). Cluster 1 comprised of 25 genes characterized by induction at Ψ_{max}, and moderate or no remission during therapy (Figures 2A and 2B). In line with the enteropathy data (Figures 1D–1H), many of these genes (e.g., *Ifng*, *Il1b*, *Tnf*, *Il6*, and *Cxcl10*) are typically induced in highly inflamed tissues. The data were corroborated by real-time qPCR assays (e.g., Figures 2C and 2D). Genes within clusters 2–4 were either mildly regulated or non-responsive (Figure S1C). Finally, principal-component analysis of the

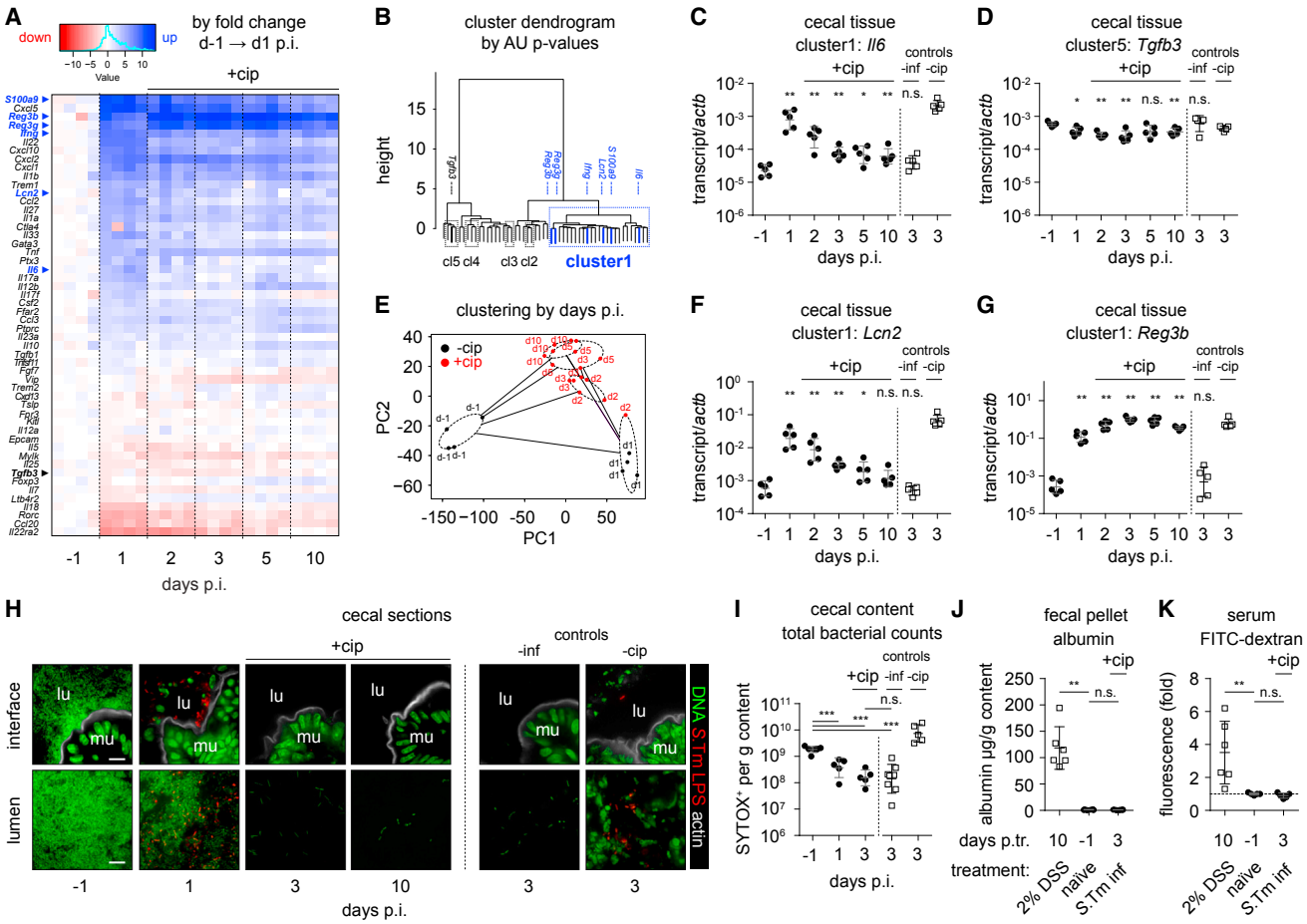

Figure 2. Mucosal Gene Expression, Microbes, and Barrier Function during Antibiotic Therapy of Acute *S*.Tm Colitis

(A) Expression heatmap of 52 pro-inflammatory and antimicrobial genes. Colors, indicate fold change of ΔC_q versus day −1; data are sorted as highest → lowest at d1 p.i.

(B) Hierarchical clustering of data from (A) (full list: Table S1).

(C and D) *Il6* (C) and *Tgfb3* (D) transcript levels.

(E) Principal component analysis of all 52 genes from naive mice (d-1; black) or mice during infection (black) and therapy (red).

(F and G) *Lcn2* (F) and *Reg3b* (G) transcript levels. Significance is tested versus d-1 (C, D, F, and G).

(H) Micrographs of cecal sections. Scale bar, 10 µm.

(I) Total bacterial density in cecal content quantified by FACS.

(J and K) Epithelial barrier function in naive and DSS-treated controls compared to infected mice after 2 days of antibiotic therapy. (J) Serum albumin in cecal content determined by ELISA. (K) FITC fluorescence in serum.

Summary graphs show five to eight individual mice pooled from two to t hree independent experiments as mean ± SD. Statistical significance was analyzed via the Mann-Whitney U test. −1, mice w/o sm, cip, or *S*.Tm; +cip, oral ciprofloxacin treatment; -inf, only treatment, no infection; -cip, only infection, no treatment; n.s., not significant; lu, lumen; mu, mucosa.

expression profiles indicated clear differences between naive mice, mice at Ψ_{max}, and mice during antibiotic therapy. Strikingly, the latter clustered together, no matter whether the therapy was applied for 1, 2, 4, or 9 days (Figure 2E). This suggested that an unresolved pro-inflammatory program persisted during the course of therapy. We reasoned that these unresolved responses might be of key importance for understanding why antibiotic treatment has proven inefficient at treating non-complicated cases of NTS diarrhea.

Interestingly, cluster 1 included several antimicrobial peptides, a fundamental arm of the mucosal innate immune defense (Bevins and Salzman, 2011). Antimicrobials secreted in high amounts are also critical biomarkers of adjunct diagnostics during infectious gastroenteritis (Figure S1D; (Gonzalez et al., 2015)). Among the antimicrobial genes of cluster 1, *S100a9* and *Lcn2* (typically expressed by polymorphonuclear cells [PMNs]) were 100- to 1,000-fold induced at Ψ_{max}. Their expression decreased significantly (though not completely) during therapy (Figures 2F and S1E). This was reminiscent of the remission kinetics shown in Figures 1E and 1G. In contrast, expression of epithelial-derived C-type lectins *Reg3b* and *Reg3g* continued to rise during the first 2 days of therapy and remained high to the end (Figures 2G and S1E). These data pointed to an underlying immune activation, which did not resolve with mucosal histopathology. Initially, we

speculated that a compromised barrier or the up-growth of unidentified microbes might be involved.

To assess microbial content, we analyzed tissue sections by SYTOX Green and anti-*Salmonella* O antigen group B antibody staining. At Ψ_{max}, high numbers of *S*.Tm were present at the mucosal interface and in the lumen (Figure 2H). Importantly, no *S*.Tm was detected within the gut lumen, and gut tissue loads were strongly reduced during therapy (Figures 1C, 2H, and S1F). SYTOX Green staining and microscopy or fluorescence-activated cell sorting (FACS) detected a dense microbial community in untreated mice, which was reduced during ciprofloxacin therapy (Figures 2H, 2I, and S1F). Among the remaining microbes, 16S sequencing did not identify species with known virulence potential (Table S2). Thus, pathobiont blooms are not a likely cause of the slow remission.

Additionally, we assessed intestinal permeability by measuring serum albumin levels in the fecal pellets, or fluorescein isothiocyanate (FITC)-dextran in the serum after oral gavage (Figure S1G). In contrast to dextran sodium sulfate (DSS)-induced colitis (positive control), *S*.Tm-infected mice did not show evidence of increased intestinal permeability at day 2 of ciprofloxacin therapy (Figures 2J and 2K). Thus, compromised barrier function does not seem to explain why appreciable levels of mucosal inflammation remain during antibiotic therapy.

Hence, other causes were likely involved. The fact that some cluster 1 genes remained highly expressed throughout the therapy suggested a role for innate mechanisms. We therefore reasoned that the cellular dynamics of myeloid infiltrates or lymphoid regulators may be a key to unravel the underlying mechanisms of remission during therapy.

The Myelomonocytic Compartment: Responders to Acute Gut Inflammation and Resolution

To evaluate the composition of myeloid cells during therapy, we used fractalkine receptor CX_3CR1-GFP reporter mice that allow detailed identification of intestinal mononuclear phagocytes (Jung et al., 2000; Tamoutounour et al., 2012). Additionally, we devised a purification procedure that allowed isolation of lamina propria cells from the cecal mucosa (1) to assess cell composition and (2) to enable intracellular detection of regulatory cytokines (see Experimental Procedures; Figure 3A; Table S3; Figures S2A and S2B).

Our analysis focused on day 2 of the therapy (day 3 p.i.), when pathogen loads are diminished and the mucosa begins to recover (Ψ_{50}). In the absence of therapy, Ly-6G$^+$ neutrophils massively accumulated in the cecal mucosa by days 1–3 p.i. (Figures 3B and 3C; Figures S2C–S2G). Importantly, antibiotic treatment reduced the abundance of these granulocytes in the cecal mucosa (Figures 3B, 3C, and S2C–S2E). Among the phagocytic mononuclear leukocytes, Ly-6C^{hi} monocyte-derived cells (MCs) were particularly prominent at day 1 p.i. (Figure 3D). In this subset of CD103$^-$ CX_3CR1^+ myeloids, we observed pronounced differentiation into Ly-6C$^+$ MHCII$^+$ (MC^{int}) and Ly-6C$^-$ MHCII$^+$ macrophages (mac; Figures 3D and 3E), a process dubbed as the "monocyte waterfall" (Figures 3A, S2H, and S2I) (Tamoutounour et al., 2012). The abundance of the inflammatory MC^{int} cells was significantly reduced after 2 days of antibiotic therapy (Ψ_{50}), and this coincided with the accumulation of differentiated Ly-6C$^-$ MHCII$^+$ mac (Figures 3D and 3E). A high proportion of MHCII$^+$ mac was also observed in the resting cecal mucosa, though at much lower numbers of CD103$^-$ CX_3CR1^+ myeloids (Figures 3A and 3E). These MHCII$^+$ mac belong to the tissue-resident mononuclear phagocyte system (MPS) that are known to maintain homeostasis in the resting gut mucosa (Bain and Mowat, 2011). Thus, the composition of PMN and MC-derived myeloids in the resolving cecal mucosa were in line with the histopathology time course (Figures 1F and 1G), suggesting that these cell populations began to normalize and slowly return to the situation of the unperturbed gut (Figures 3B–3E).

Next, we analyzed the functional properties of cecal mononuclear phagocytes (MNPs). To date, two distinct functional states of macrophage activation have been recognized. Microbial moieties and T_h1 cytokines, like IFN-γ, polarize macrophages toward an M1 phenotype associated with NF-κB and STAT1 signaling that boosts expression of the chemokines CXCL9-10, the cytokines interleukin-1β (IL-1β), and tumor necrosis factor (TNF). In contrast, tissue remodeling during wound healing is orchestrated by M2 macrophages requiring PPAR-γ and Stat6 signaling (Murray and Wynn, 2011). While freshly extravasated blood monocytes create a highly antimicrobial and inflammatory M1-like environment, resident intestinal macrophages are clearly different from the M1 and M2 populations as they are highly phagocytic and do not express arginase, and an essential source of IL-10 (Bain and Mowat, 2011). To assess such functional phenotypes of MNPs during remission, we measured the overall transcript levels of the M1-type signals *Il1b*, *Tnf*, and *Nos2* in the cecal tissue. The infection with *S*.Tm drastically increased the expression of these mediators at day 1 p.i. (Figures 3F and S2J). After two days of antibiotic therapy, *Il1b* and *Tnf* levels declined by >2-fold (Figure 3F), while the expression of *Nos2* remained unchanged (Figure S2J). To study this in more detail, highly purified CD11b$^+$ CX_3CR1^+ myeloid cells were isolated by cell sorting and analyzed by real-time qPCR. After 2 days of antibiotic therapy, *Il1b* and *Tnf* expression by CX_3CR1^+ MNPs declined, while the expression of *Nos2* and the anti-inflammatory *Il10* increased (Figure 3G). This verified that the resolving cecal mucosa accumulates Ly-6C$^-$ MHCII$^+$ intestinal macrophages, which are characteristic for mucosal homeostasis (Figures 3A and 3E).

In a complementary approach, we analyzed mucosal STAT1 signaling that regulates pro-inflammatory M1 activity. Immunohistochemistry of cecal tissue sections revealed that *S*.Tm boosts phosphorylated STAT1 levels by day 1 p.i., in particular in cells of the lamina propria (red arrowheads; Figure 3H). Quantitative western blot analysis confirmed that pY701 STAT1 highly accumulated by day 1 p.i., while antibiotic therapy reduced the relative abundance of pY701 in the gut mucosa (Figure 3I). These data are consistent with our hypothesis that antibiotic therapy results in a significant, but incomplete restoration of MNP homeostasis. However, it remains to be shown how this may affect remission kinetics.

Extent of Resolution Is Controlled by an IFN-γ-Dependent Program

The factors controlling mucosal recovery during antibiotic therapy remains to be identified. We speculated that two different phenomena might be involved: (1) persistent bacteria, which

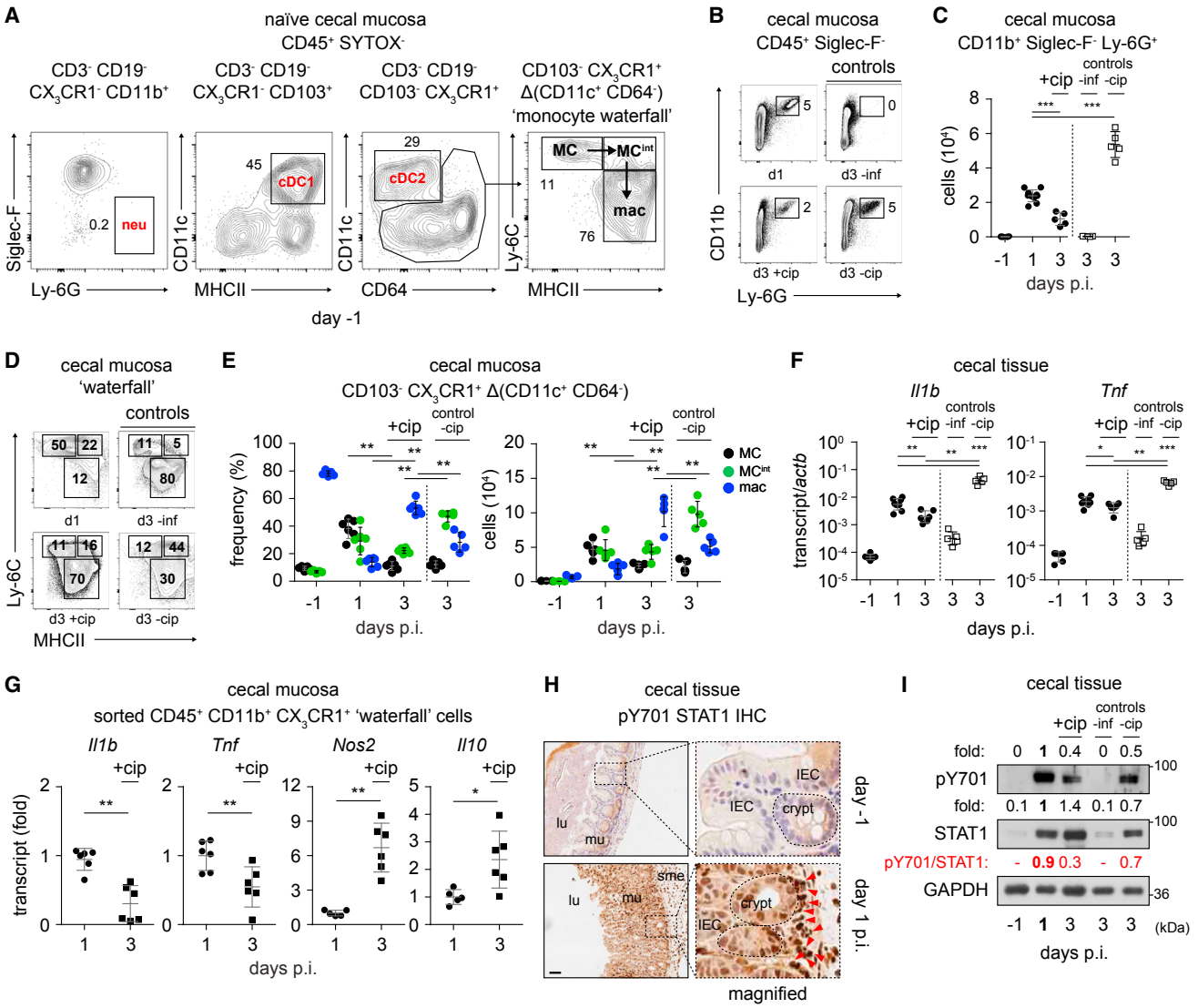

Figure 3. Mucosal Myeloid Responses during Acute Gut Inflammation and Antibiotic Therapy

(A–E) CX_3CR1-GFP mice were infected as in Figure 1. (A) Myeloid subsets in the naive cecal mucosa. (Full list is shown in Table S3.) (B and C) Ly-6G$^+$ neutrophils. (D and E) Monocyte waterfall cells. MC: Ly-6C^{hi} MHCII$^-$ → MC^{int}: Ly-6C$^+$ MHCII$^+$ → mac: Ly-6C$^-$ MHCII$^+$.

(F) *Il1b* and *Tnf* transcript levels.

(G) *Il1b*, *Tnf*, *Nos2*, and *Il10* transcript levels of purified CD11b$^+$ CX_3CR1^+ cells.

(H) Phospho-STAT1 (Y701) immunohistology of cecal tissue sections. Red arrowheads: lamina propria cells. Scale bar, 50 μm.

(I) Western blot analysis of pY701 STAT1, STAT1, and GAPDH. 0, below detection limit.

Summary graphs show five to seven individual mice pooled from two to five independent experiments as mean ± SD. Statistical significance was analyzed via the Mann-Whitney U test. neu, neutrophil; cDC, type 1/2 conventional dendritic cell; MC, monocyte-derived cell; mac, macrophage; MC^{int}, MC-mac intermediate; −1, mice w/o sm; +cip, oral ciprofloxacin treatment; -inf, only treatment, no infection; -cip, only infection, no treatment; lu, lumen; mu, mucosa; sme, submucosal edema.

survive the antibiotic therapy in the gut tissue (Diard et al., 2014; Kaiser et al., 2014), might elicit sustained pro-inflammatory responses and thereby delay remission, or (2) an unidentified program of the mucosal immune system that hinders resolution kinetics independent of pathogen loads.

First, we determined the number of persistent bacteria that survive in the cecum tissue during ciprofloxacin therapy. Plating and microscopic enumeration of intracellular bacteria residing in the cecal mucosa established that *S*.Tm tissue loads were reduced by 50- to 1,000-fold during therapy (Figures 4A and 4B). Further reducing the load of *S*.Tm persisters by combined therapy (i.e., by treating with a second antibiotic, ceftriaxone) did not enhance resolution (Figures 4E–4J). Thus, persistent pathogen cells remaining in the gut tissue do not seem to limit remission kinetics during ciprofloxacin therapy.

To pinpoint potential molecular candidates that may delay remission, we performed a volcano plot analysis of the cecal mucosa transcriptional profiles from Figures 2A and 2B. Transcripts

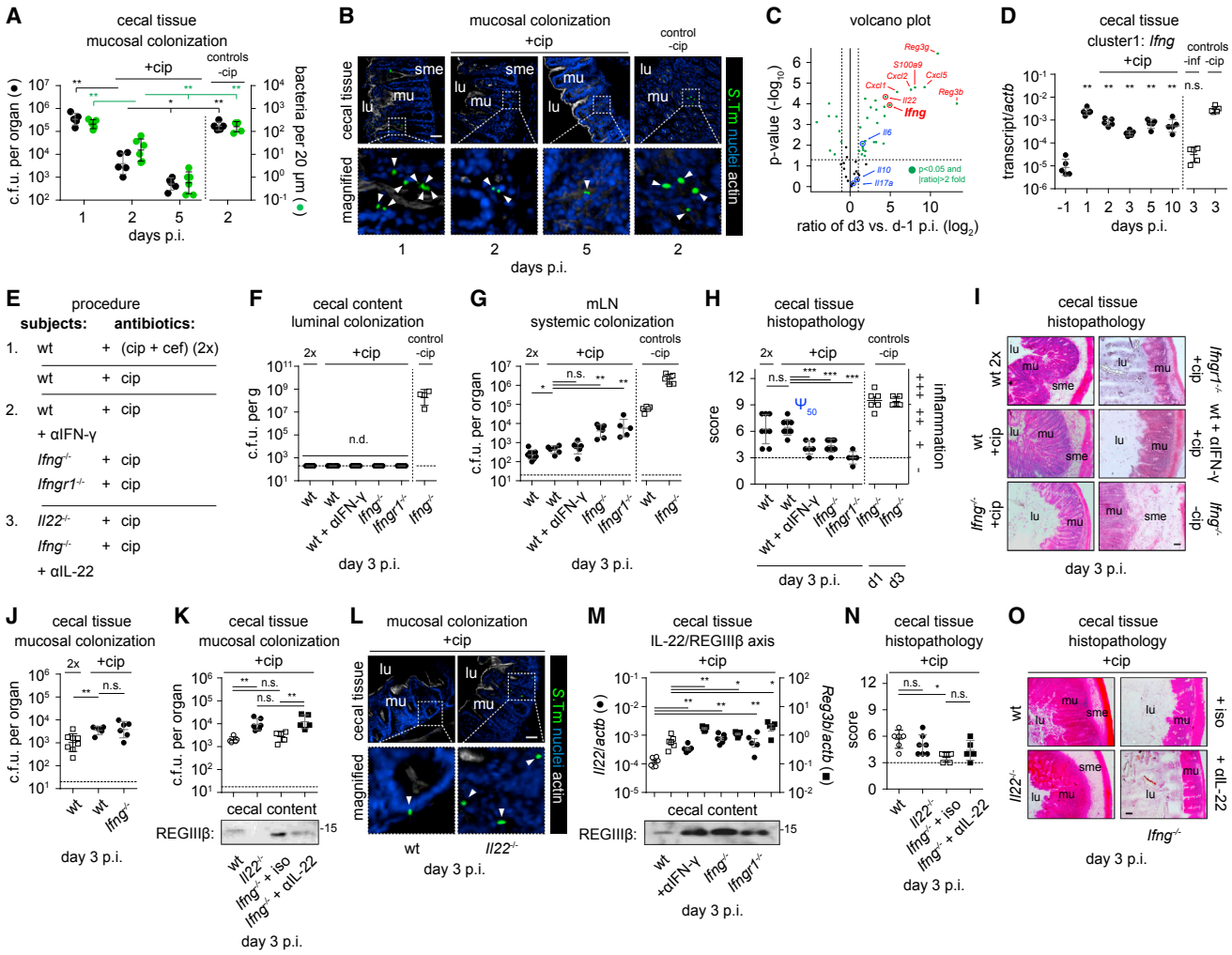

Figure 4. IFN-γ Hinders Mucosal Remission

(A and B) *S*.Tm tissue load determined by plating (black) or fluorescence microscopy (green). Scale bar, 50 μm.

(C) Volcano plot analysis of Figure 2A data correlating relative expression and significance. Red, top eight hits.

(D) *Ifng* transcript levels. Significance was assessed versus d-1.

(E) Tested experimental groups in (F)–(O).

(F) *S*.Tm loads in cecal content.

(G) *S*.Tm loads in mesenteric lymph nodes.

(H and I) Histopathology scoring of cecal tissue. Scale bar, 100 μm.

(J and K) *S*.Tm tissue load determined by plating.

(L) *S*.Tm tissue load depicted by fluorescence microscopy. Scale bar, 50 μm.

(M) *Il22* and *Reg3b* transcript levels.

(K and M) REGIIIβ as detected in cecum content by western blots.

(N and O) Histopathology scoring of cecal tissue. Scale bar, 100 μm.

Summary graphs show five to eight individual mice pooled from two to five independent experiments as mean ± SD. Statistical significance was analyzed via the Mann-Whitney U test. −1, mice w/o sm; +cip, oral ciprofloxacin treatment; -inf, only treatment, no infection; -cip, only infection, no treatment; n.s., not significant; cef, ceftriaxone treatment; αIFN-γ, αIL-22, neutralizing antibodies; lu, lumen; mu, mucosa; sme, submucosal edema.

remaining at a relatively high level at Ψ_{50} included CXCL-chemokines, AMPs, as well as IFN-γ and IL-22. In fact, IFN-γ was the most prominent cytokine at the transcriptional level by day 3 and 5 p.i. (Figures 4C and S3A). It showed a typical cluster 1 signature with >100-fold induction at day 1 p.i. and sustained high expression remaining at least 30-fold above the homeostatic level during the course of therapy (Figure 4D). To assess whether IFN-γ might limit remission kinetics, we determined resolution indices in the face of compromised IFN-γ signaling (i.e., in *Ifng*$^{-/-}$ or *Ifngr1*$^{-/-}$ mice), or alternatively by antibody-mediated IFN-γ neutralization during ciprofloxacin therapy (Figure 4E). While IFN-γ deficiency did not affect antibiotic-mediated clearance of gut luminal bacteria, it resulted in elevated loads of persistent bacteria at systemic sites in genetically susceptible *Ifng*$^{-/-}$ and *Ifngr1*$^{-/-}$ mice (Figures 4F and 4G). Surprisingly, this was not observed in mice treated with ciprofloxacin and

IFN-γ-neutralizing antibodies (Figure 4G). We speculate that IFN-γ is critical during the first day to restrict pathogen trafficking to systemic sites. Most importantly, however, mucosal inflammation was reduced in all groups of IFN-γ-impaired animals (Figures 4H and 4I). The expression of characteristic pro- or anti-inflammatory mediators (e.g., *Il6*, *Il17a*, *Il10*) remained unchanged and IL-10 deficiency did not affect mucosal inflammation (Figures S3C–S3F). Thus, it remained unclear how IFN-γ affects remission.

First, we determined persistent bacterial loads in the IFN-γ impaired mucosa. *Ifng*$^{-/-}$ animals, despite featuring elevated counts in the mesenteric lymph node (mLN) (Figure 4G), had equivalent gut tissue loads compared to WT mice (Figure 4J). We speculated that the effect of such tissue-specific pathogen control might root in the regulation of antimicrobial host defenses. While the mucosal expression of *S100a9* showed no significant difference (Figure S3G), REGIIIβ expression was further elevated in the absence of IFN-γ signaling (Figure 4M). These data suggested that epithelial REGIIIβ levels may compensate for the reduced antimicrobial activity of myeloid cells (that is typically observed under systemic IFN-γ deficiency) and thereby explain why mucosal pathogen loads of WT and IFN-γ-deficient mice do not differ after 2 days of ciprofloxacin therapy.

Next, we assessed IL-22. Lymphoid cell-derived IL-22 is a key regulator to boost the expression of REGIII family C-type lectins (which can limit *S*.Tm growth; Figure S3, legend) in the gut and the lung epithelium (Sonnenberg et al., 2011). Accordingly, IL-22-deficient animals featured reduced levels of REGIIIβ and increased pathogen loads in the cecal mucosa at Ψ_{50} (Figures 4K–4L). Interestingly, we found elevated levels of *Il22* and *Reg3b* expression in the cecal mucosa of IFN-γ-impaired mice (Figure 4M). Although the cellular source of mucosal IL-22 during oral *Salmonella* infection is yet poorly defined, the contribution of CD3$^+$ T cells during later stages of acute inflammation has been reported (Godinez et al., 2008). To this end, we observed that the IFN-γ-deficient cecal mucosa harbored increased proportions of IL-22-producing Thy1$^+$ CD3$^+$ γδ T cells (Figures S3H–S3M). Next, we analyzed whether IL-22 deficiency would affect resolution kinetics. While the IL-22/REGIII antimicrobial axis was clearly involved in mucosal pathogen control during therapy, we observed no significant difference in the pathology of antibiotic-treated mice under IL-22-sufficient or -deficient conditions (Figures 4N–4O). These data suggest that IFN-γ has two effects during antibiotic therapy, i.e., delaying resolution of mucosal inflammation and coordinating pathogen restriction at systemic sites, where genetic IFN-γ deficiency permits higher persister loads. The gut mucosa might remain protected by (compensatory) epithelial IL-22/REGIII responses even in IFN-γ-deficient mice. The cellular source of mucosal IFN-γ and its downstream mechanism of regulation remain, however, to be elucidated.

Impaired IFN-γ Signaling Promotes Granulocyte and Macrophage Plasticity during Therapy

IFN-γ is an important stimulus for immune activation and differentiation. We therefore asked how IFN-γ would affect cecal lamina propria myeloid cell composition. In line with the accelerated remission kinetics, mice with compromised IFN-γ signaling harbored reduced Ly-6G$^+$ neutrophil numbers in the cecal mucosa after 2 days of therapy (Figures 5A and 5B). The proportion of Ly-6C$^+$ MHCII$^+$ MC^{int}, another archetypal subset of severe acute inflammation, was also reduced (Figures 5C and 5D). This went along with the accumulation of differentiated Ly-6C$^-$ MHCII$^+$ mac, a cell type typically observed in homeostasis and advanced remission. We therefore speculated that the resolving histopathology observed under paucity of IFN-γ is in fact related to the described plasticity of myeloids.

Next, we asked whether there was a functional link between IFN-γ signaling and mucosal MNP activity during remission. Indeed, transcript levels of IL-1β, TNF, and iNOS were significantly lowered in *Ifng*$^{-/-}$, *Ifngr1*$^{-/-}$ or IFN-γ-neutralized animals (Figures 5E and 5F). This went along with reduced levels of total STAT1 proteins without detectable pY701 (Figure 5G). Furthermore, IFN-γ deficiency boosted the expression of *Arg1* and *Retnla*, which are hallmarks of a transcriptional program determining M2 macrophage identity in wound healing and tissue repair (Figure 5H; Murray and Wynn, 2011). These observations would further support that IFN-γ delays remission by hindering the shift from inflammatory back to homeostatic myeloids and the concomitant removal of pro-inflammatory mediators.

Contribution of IFN-γ-Producing Lymphoid Cells to Delayed Recovery in Antibiotic-Treated Mice

Next, we aimed to define the cellular origin of mucosal IFN-γ production. Detailed analysis of the CD45$^+$ Thy1$^+$ mucosal compartment revealed two distinct IFN-γ$^+$ subsets after 2 days of therapy (Figures 6A and S4A). IFN-γ-producing CD3$^+$ CD11b$^-$ cells were mainly β TCR$^+$ T cells that expressed CD8α, CD8β, and CCR6, overall indicating an intraepithelial lymphocyte phenotype (Figure 6B). Some IFN-γ$^+$ T cells also expressed γδ TCR and NK1.1, indicating that NKT cells do also contribute (Figure 6B). IFN-γ-producing CD3$^-$ CD11b$^+$ cells on the other hand were predominantly classified as NK1.1$^+$ Eomes$^+$ NK cells with an activated DX5$^+$ CD27$^+$ phenotype (Figure 6C). Absolute quantification within the total CD45$^+$ Thy1$^+$ IFN-γ$^+$ pool revealed that the IFN-γ$^+$ T cells were more abundant than the NK cell subset in the cecal mucosa during resolution (Figure 6D).

To evaluate the contribution of these IFN-γ-producing subsets to delaying mucosal remission, we analyzed (1) animals in which NK1.1-expressing cells were depleted during therapy (to eliminate CD3$^+$ NKT and CD3$^-$ NK cells), or (2) *Tcrbd*$^{-/-}$ mice genetically lacking CD3$^+$ T cells, or (3) mice in which NK1.1-expressing cells were depleted on a *Tcrbd*$^{-/-}$ background. Importantly, depletion of NK1.1$^+$ cells only minimally altered the frequency of IFN-γ$^+$ CD3$^+$ cells (Figure S4B), while lack of the T cell compartment in *Tcrbd*$^{-/-}$ mice did not affect the pool of CD11b$^+$ NK cells (Figure S4C). This suggested that the two main subsets of IFN-γ producers can be studied separately from each other. Next, we asked whether reduction in CD11b$^+$ NK cell numbers or the lack of CD3$^+$ T cells affected the resolution of inflammation during therapy. Neither depletion of NK1.1$^+$ cells nor T cell deficiency alone was sufficient to alter remission kinetics at Ψ_{50} (Figures 6E and 6F). Strikingly, when NK1.1$^+$ cells were depleted on a *Tcrbd*$^{-/-}$ background, the animals consistently featured reduced mucosal pathology (Figures 6E and 6F). This penocopied the *Ifng*$^{-/-}$ mice (Figures 4H and 4I).

In earlier work, we had found that IFN-γ signaling controls mucus excretion, presumably by signaling via the goblet cells'

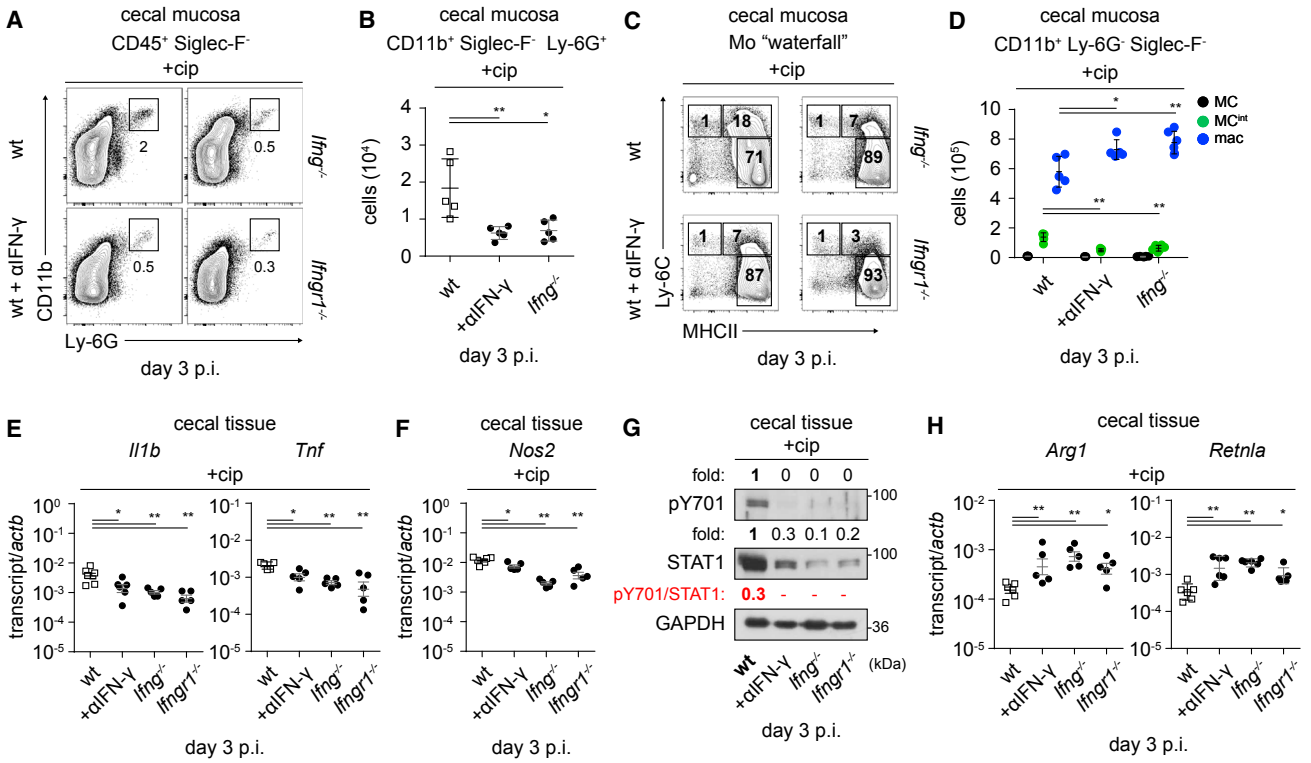

Figure 5. Ablation of IFN-γ Signaling Promotes Myeloid Plasticity

Bl6 and knockout mice were infected as in Figure 4E.

(A and B) Ly-6G$^+$ neutrophils.

(C and D) Monocyte waterfall cells. MC: Ly-6C^{hi} MHCII$^-$ → MC^{int}: Ly-6C$^+$ MHCII$^+$ → mac: Ly-6C$^-$ MHCII$^+$.

(E and F) *Il1b*, *Tnf* (E), and *Nos2* (F) transcript levels.

(G) Western blot analysis of pY701 STAT1, STAT1, and GAPDH. 0, below detection limit.

(H) *Arg1* and *Retnla* transcript levels.

Summary graphs show five to six individual mice pooled from two to three independent experiments as mean ± SD. Statistical significance was analyzed via the Mann-Whitney U test. +cip, oral ciprofloxacin treatment.

IFNGR (Songhet et al., 2011). This was used as a readout for probing the intensity of mucosal IFN-γ signaling during antibiotic therapy. WT animals displayed lower numbers of mucus-filled vacuoles than NK-cell-depleted *Tcrbd*$^{-/-}$ mice (Figure 6G). Moreover, the lamina propria of these mice featured reduced numbers of Ly-6G$^+$ cells, and the cecal mucosa expressed less *Il1b* (Figures 6H and 6I). Put together, this identifies IFN-γ-producing T, NKT, and NK cells as key players with partially redundant function that control the kinetics of mucosal remission from acute diarrhea during antibiotic therapy.

DISCUSSION

The mechanisms controlling re-establishment of homeostasis after microbial gut infections still remain elusive. A better understanding of the temporal and molecular parameters of recovery from acute intestinal disease is vital and urgent, especially in therapy of immunocompromised patients and children (Saleh and Elson, 2011; Scallan et al., 2015; Schwille-Kiuntke et al., 2015). Here, we analyzed remission during antibiotic therapy in an acute *S.* Typhimurium enterocolitis model. High-dose ciprofloxacin therapy efficiently eliminates the pathogen from the gut lumen, while ~1%–10% of the bacteria survive in an antibiotic-tolerant state within the intestinal tissue and the mLN. Significant (though incomplete) remission of mucosal pathology occurs during the first 2 days of antibiotic therapy, reducing the inflammation by about 50% (Ψ_{50}). The restoration of epithelial integrity (Figures 2H, 2J, and 2K) seems to precede the clearance of highly accumulated PMNs (Figures S2C, 2F, S1D, and S1E) and the restoration of homeostatic non-inflammatory MNP populations (Figures 3D–3I). Remission kinetics at this stage are limited by IFN-γ released from mucosal T and NK cells. Strikingly, ablation of IFN-γ signaling (1) accelerated the clearance of neutrophils, (2) promoted the maturation and polarization of intestinal MNPs toward homeostasis, (3) attenuated STAT1 signaling, and (4) boosted the antimicrobial host defense via IL-22/REGIIIβ. These findings may explain why antibiotics fail to relieve enteropathy in human patients (Onwuezobe et al., 2012). Moreover, such IFN-γ dependent mechanisms may be of broad relevance to other pathogenic infections (Burrack and Morrison, 2014; Chiang et al., 2012) and other inflammatory disorders such as allergy, renal fibrosis, neurodegenerative diseases, or cancer (Janakiram et al., 2011; Levy and Serhan, 2014; Luo et al., 2013).

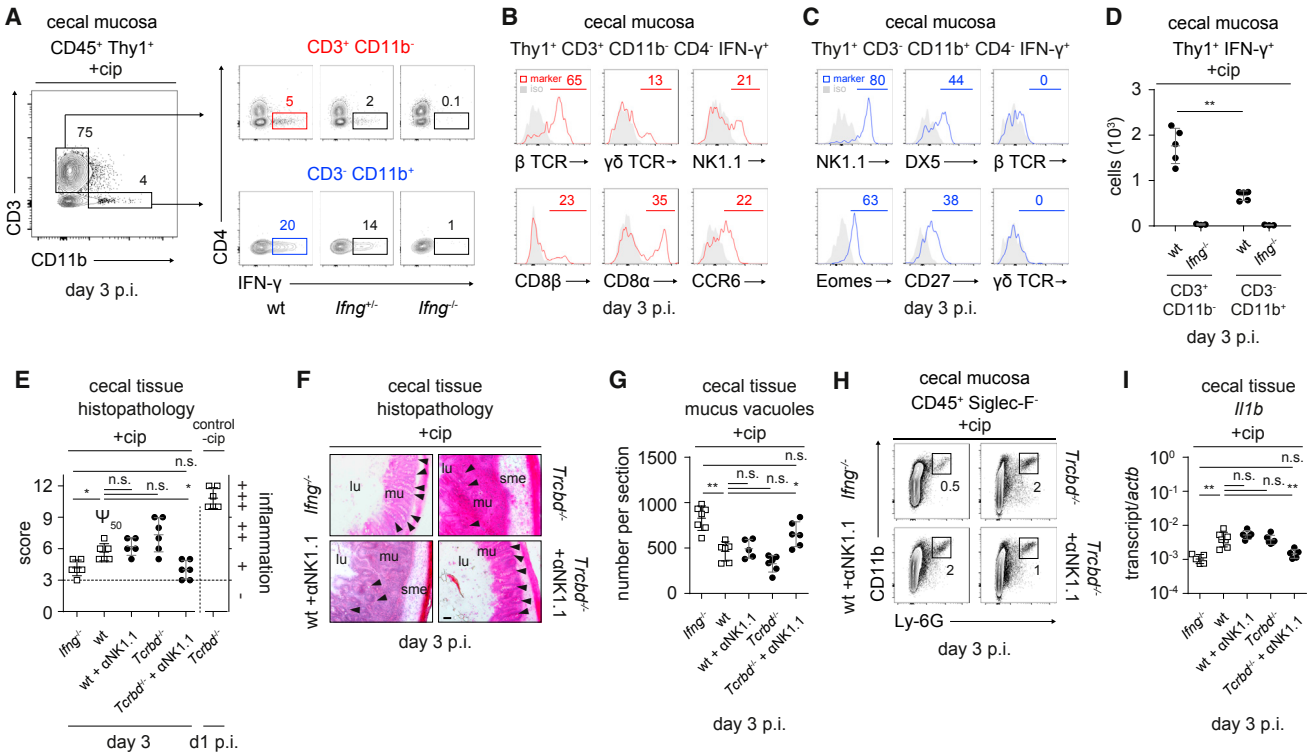

Figure 6. IFN-γ-Producing Lymphoid Cells Delay Remission in Antibiotic-Treated Mice

(A–D) Mice were infected as in Figure 4E. IFN-γ production (A and D) and surface marker expression by (B) $CD3^+$ $CD11b^-$ and (C) $CD3^-$ $CD11b^+$ cells.

(E–I) Bl6 or *Tcrbd*$^{-/-}$ mice were infected as in Figure 1 and additionally treated with αNK1.1-depleting antibodies during therapy, as indicated. (E) Histopathology scoring of cecal tissue. (F) H&E-stained cecal tissue sections. Scale bar, 100 μm. (G) Mucus-filled vacuole retention (black arrowheads). Sections originate from Figures 6E and 6F. (H) Ly-$6G^+$ neutrophils. (I) *Il1b* transcript levels.

Summary graphs show five to seven individual mice pooled from two to three independent experiments as mean ± SD. Statistical significance was analyzed via the Mann-Whitney U test. +cip, oral ciprofloxacin treatment; n.s., not significant; αNK1.1, depleting antibody for $NK1.1^+$ cells.

Bacterial infections and food-borne diarrhea continue to cause significant morbidity and mortality worldwide (GBD 2013 Mortality and Causes of Death Collaborators, 2015). In fact, diarrheal diseases rank among the top 10 causes of 'loss in disability-adjusted life years' (DALY; Murray et al., 2015), and non-typhoidal *Salmonella* spp. belong to the most prominent food-borne agents across the globe (Kirk et al., 2015). Strikingly, people recovering from the initial, acute disease are prone to continued sequelae, explaining the high disease burden inflicted by diarrheal diseases. The underlying mechanisms are not yet well understood. Our findings indicate that antibiotic therapy of murine *S*.Tm enterocolitis might offer a model to study such mechanisms. In this model, the pathogen is eliminated from the lumen as early as 3 hr after treatment (Kaiser et al., 2014), while complete resolution is only achieved by 7–9 days of therapy (Figure 1G). Molecular inspection unraveled that a set of genes remained highly expressed throughout the treatment (Figures 2A and 2E). We refuted a role for (1) residual luminal *S*.Tm that may provoke sustained immune activation at the mucosal interface (Figures 1C, 2H, and S1F); (2) blooms of pathogenic members of the residential microbial community (Figures 2I, S1F, S5A, and S5B; Table S2); and (3) prolonged gut barrier dysfunction (Figures 2J and 2K) as implicated in chemical colitis (Wirtz et al., 2007). Much rather, residual inflammation well after antibiotic-mediated pathogen-clearance resulted (at least in part) from IFN-γ-dependent immune dysregulation. It is tempting to speculate that this mechanism may enhance susceptibility to subsequent infections (Osborne et al., 2014) and/or contribute to the high prevalence of "post-infection" gastrointestinal disorders, such as irritable bowel syndrome (Koh et al., 2012).

To address what elicits the pro-inflammatory program sustaining mucosal inflammation, we speculated that persistent *S*.Tm surviving in the tissue of antibiotic-treated mice might be involved. Indeed, such persisters have been identified (Claudi et al., 2014; Diard et al., 2014). In line, about 1% of bacteria survived therapy within the mucosal tissue by day 5 p.i. (Figures 4A and 4B). As *S*.Tm persisters are predominantly lodged within patrolling $CD11c^+$ MNPs (Helaine et al., 2014; Kaiser et al., 2014), we initially hypothesized that these persisters may stimulate the residual inflammation and that this may cease if persisters were eliminated. We found, however, that resolution kinetics were left unchanged if persister loads were lowered by combined antibiotic treatment (Figures 4H and 4I; Figure S5C), or increased in mice with impaired antimicrobial host defense during early recovery (Figures 4K–4O). Thus, 10-fold changes in persister loads do not seem to affect resolution kinetics. However, this cannot formally rule out that (besides IFN-γ) persisters may also contribute to slowing down remission.

While IFN-γ is induced by >100-fold during the first day of infection, possibly to modulate innate MNP function, its release from mucosal T and NK cells was found to delay resolution. This was supported by several lines of evidence. (1) IFN-γ was dispensable for mounting mucosal inflammation at day 1 p.i. (Figure 4H; A.A.M., unpublished data); (2) cytokine neutralization during therapy resulted in comparable resolution kinetics as observed in mice with genetic IFN-γ defficiency (Figures 4E–4I and 5); (3) reduced IFN-γ levels attenuated canonical STAT1 signaling (Figure 5G); and (4) cytokine deficiency permitted mucosal remodeling of Ly-6G$^+$ neutrophils and intestinal MNPs (Figure 5). These findings are in line with previous studies implicating IFN-γ in disease resolution and tissue scarring in *Chlamydia* trachoma (Hu et al., 2013), STAT1-associated pathophysiology in ulcerative colitis (Schreiber et al., 2002), tissue-specific cytokine patterns in remissive pediatric Crohn's disease (Agnholt et al., 2003; Sylvester et al., 2014), and retuned responsiveness of macrophages in respiratory exacerbations (Kaur et al., 2015). While IFN-γ is clearly important, we cannot exclude that other factors (e.g., TNF, IL-6, IL-17A), the remaining persisters or (at later stages) adaptive immune responses may also affect remission. Our data would also be in line with compromised migratory CD103$^+$ DC function observed in severe long-term lymphadenopathy after acute *Y. pseudotuberculosis* infection (Fonseca et al., 2015).

Together, our study explains why mucosal inflammation may remain during antibiotic therapy and provides key insights into how the innate immune system reshapes the mucosal milieu after acute NTS challenge. Monitoring of pathogen shedding is clearly insufficient for probing the resolution of disease and should be supplemented by data on key inflammatory markers like IFN-γ. Such improved diagnostic protocols would seem pivotal for analyzing remission in human patients, in particular, in cases with sustained enteropathy. Understanding the mechanisms that drive remission to homeostasis will enable a next generation of therapeutic approaches that may combine antibiotics with the boosting of cell-mediated cytotoxicity (Maltez et al., 2015) and/or the collateral resolution of inflammatory mediators.

EXPERIMENTAL PROCEDURES

Animals

C57BL/6J SFP, C57BL/6J GNO, B6.129P-*Cx3cr1*^{tm1LittJ}, B6.129S7-*Ifng*^{tm1Ts}/J, B6.129S5-*Il22*^{tm1Lex}; B6.129P2-*Tcrb*^{tm1Mom}*Tcrd*^{tm1Mom}/J; B6.129S7-*Ifngr1*^{tm1Agt}/J mice were housed and bred under SPF conditions in individually ventilated cages (IVCs) in RCHCI and EPIC, ETH, Zürich, and in LASC, UZH, Zürich, respectively. Mice were used at an age of 6–12 weeks, and *Ifng*$^{-/-}$ or *Il22*$^{-/-}$ animals included littermates. All animal procedures have been performed as approved by the Kantonales Veterinäramt (223/2010, 222/2013).

Infections, Bacteria, Antibiotic Therapy, and Antibody Treatment

Mice were orally pre-treated with 20 mg streptomycin (Applichem) and infected with SB300, a wild-type *Salmonella enterica* ssp. *enterica* serovar Typhimurium SL1344 derivative (Barthel et al., 2003). Ciprofloxacin (Ciproxine 500 mg, Bayer) was applied in 2.5-mg dosage per os twice daily ("+cip"; Kaiser et al., 2014). Ceftriaxone (Rocephin 1 g, Roche) was supplemented daily 1.25 mg intraperitoneally (i.p.). Of note, 12 hr after the first antibiotic treatment, animals were transferred into fresh cages to avoid re-contamination via the oral route. Bacterial loads in stool and organs were determined by plating on MacConkey agar (Oxoid; 50 μg/ml streptomycin). Cecal tissue lysates were prepared after 30 min incubation in 400 μg/ml gentamycin/PBS and six subsequent washes in PBS. Anti-IFNγ (Bio X Cell; R4-6A2; 500 μg twice daily), anti-IL-22 (eBioscience; IL22JOP; 500 μg once), rat IgG2a κ (eBioscience; 500 μg once), and anti-NK1.1 (Bio X Cell; PK136; 250 μg daily); antibodies were administered i.p. during ciprofloxacin therapy.

Histopathology and Immunohistochemistry

Ceca were excised at the entry of the ileo-cecal junction and weighed. The cecal index was defined as (total body weight)/(organ weight). Cecal tissue was frozen in Tissue Tek OCT medium (Sysmex). 10-μm cryo-sections were H&E stained using COT 20 (Medite). Pathology was scored in a blinded fashion (Barthel et al., 2003). The severity is indicated as uninflamed (–), mild (+), moderate (++), and profound (+++) colitis. For Tyr701-pSTAT1 staining (Cell Signaling Technology), tissue samples were fixed in 4% paraformaldehyde for 5 days at room temperature and embedded in paraffin. Approximately 2-μm tissue sections were deparaffinized, rehydrated, and boiled at 100°C with EDTA for antigen retrieval. Immunohistochemistry (IHC) staining was done on an automated BOND-MAX stainer using the Bond Polymer Refine Detection kit (Leica).

In Vivo Epithelial Barrier Permeability

DSS controls received 2% DSS (TdB Consultancy) in drinking water as described (Wirtz et al., 2007). Serum albumin was quantified from cecal content using a mouse albumin ELISA (Bethyl Laboratories), an ABTS-based substrate and spectroscopy (Spectramax Plus, Molecular Devices). 15 mg 4 kDa FITC-labeled dextran (TdB Consultancy) was applied to the same animals (Chassaing et al., 2015). FITC fluorescence intensity was measured in serum (485/535 nm; Victor 3, PerkinElmer).

Real-Time qPCR

The cecum mid-segments were rinsed in cold PBS and snap-frozen in RNAlater (QIAGEN). Flow-cytometry-sorted cells were directly processed. Total RNA was extracted via RNeasy Mini or Micro kits (QIAGEN), respectively. 1 μg RNA (Nanodrop) was reverse-transcribed using the RT^2 HT First Strand cDNA Kit (QIAGEN). Custom RT^2 Profiler PCR Arrays and Primer Assays (QIAGEN) were run with RT^2 SYBR Green ROX FAST (QIAGEN) on a 7900 HT Fast Real-Time PCR equipped with an SDS 2.2.1 software (Applied Biosystems). Relative transcript levels were normalized to *Actb*. The upper limit of C_q was fixed to 35 cycles. All procedures were performed according to the manufacturer's instructions. Hierarchical clustering identified gene clusters with similar expression trends using "ward" as the clustering method and "correlation" as a measure of distance. 1,000 bootstrap replicates were generated and the five clusters were determined at 0.05 significance level.

Confocal Microscopy

If indicated, animals were infected with WT *S*.Tm harboring P*ssaG-gfp* (Hapfelmeier et al., 2005). Sample preparation and confocal microscopy were performed as described (Stecher et al., 2007). Sections were stained with SYTOX Green (Life Technologies), α-*S*.Tm LPS O-antigen group B factor (Difco Laboratories), goat α-rabbit-Cy3 (Jackson ImmunoResearch Laboratories), AF647-conjugated phalloidin (Molecular Probes), or DAPI (Sigma). A Zeiss Axiovert 200-m microscope with 10×–100× objectives, a spinning disc confocal laser unit (Visitron) and two Evolve 512 EMCCD cameras (Photometrics) were used for image recording, and Visiview (Visitron) for image analysis. *S*.Tm P*ssaG-gfp* was manually enumerated as GFP$^+$ intracellular events in six to nine non-consecutive 20-μm sections for each animal analyzed.

Cecal Lamina Propria Cell Isolation, Antibodies, and Flow Cytometry

Excised ceca were opened longitudinally, placed into 4°C PBS, and briefly vortexed. Tissues were cut into pieces and incubated twice in 5 mM EDTA, 15 mM HEPES, 10% fetal calf serum (FCS) in PBS for 20 min at 37°C, while mildly shaking at 120 rpm. Samples were rinsed in RPMI (30% FCS), further sliced, and digested for 60 min in RPMI (Bioconcept; 1 mg/ml Collagenase VIII [Sigma], 0.2 mg/ml DNase I [Roche]). Cells were passed through a 70-μm cell strainer (BD Biosciences), rinsed in RPMI, layered onto a NycoPrep 1.077 matrix (Progen), and centrifuged for 30 min at 400 × *g*. The interface was collected, washed with RPMI, and stained in 4°C PBS (10% FCS, 0.02% NaN_3). For detecting intrinsic cytokine production, isolated cells were cultured for 5 hr in IMDM (Life Technologies; 10 μg/mL Brefeldin-A, 10%

FCS, 10 mM HEPES, 2 mM L-Glu, P/S). For intracellular cytokine detection, the Foxp3 Staining Buffer Set (eBioscience) was used. Antibodies were from BioLegend (CD45 [clone 30-F11], CD11b [M1/70], Thy1.2 [30-H.12], CD3 [17A2], CD4 [RM4-5], CD19 [6D5], TCR β [H57-597], TCR γδ [GL3], CD64 [X54-5/7.1], CD11c [N418], MHCII [M5/114.15.2], Ly-6C [HK1.4], CD103 [2E7], Ly-6G [1A8], IFN-γ [XMG1.2], NK1.1 [PK136], CD8α [53-6.8], CD8β [YTS156.7.7], CCR6 [29-2L17], CD49b [DX5], CD27 [LG.3A10]), from BD Biosciences (Siglec-F [E50-2440], Ly-6C [AL-21]), or from eBioscience (Eomes [Dan11mag]). For live-cell labeling, SYTOX or LIVE/DEAD fixable dead cell stains (Invitrogen) were included. Fc receptors were blocked with purified anti-CD16/32 (clone 93). For quantitative analysis of the intestinal microbiota, cecal contents were homogenized in PBS, snap-frozen, and subsequently labeled with SYTOX Green (Life Technologies) and, if needed, with α-*S*.Tm LPS O-antigen group B factor (Difco) and goat α-rabbit-Cy5 (Jackson ImmunoResearch). All data were acquired on a LSRII flow cytometer (BD Biosciences) and analyzed with FlowJo software (Tree Star). Calculated total luminal *S*.Tm numbers were finally normalized to input content weight.

Western Blot

REGIIIβ proteins were detected in cecal contents as described (Stelter et al., 2011). For STAT1 quantification, cecal tissue samples of equivalent weight were homogenized in 1X reducing loading buffer (Red Loading Buffer Pack, Cell Signal) supplemented with protease inhibitor cocktail tablets (Roche). Nitrocellulose membranes (Whatman) were developed using polyclonal rabbit α-RegIIIβ antibody, rabbit α-phospho-STAT1 (Tyr701), rabbit α-STAT1 (Cell Signal), rabbit α-GAPDH (Sigma), donkey α-rabbit-peroxidase conjugates (GE Healthcare), and ECL kits (GE Healthcare). Commercial antibodies were applied according to the manufacturers' instruction. ImageJ ×64 was used for analysis.

Statistical Analysis

Statistical analyses were performed using non-parametric Mann-Whitney U test. Tests were not significant $p \geq 0.05$ or significant $^{*}p < 0.05$, $^{**}p < 0.01$, $^{***}p < 0.001$.

SUPPLEMENTAL INFORMATION

Supplemental Information includes Supplemental Experimental Procedures, five figures, and three tables and can be found with this article online at http://dx.doi.org/10.1016/j.chom.2016.06.008.

AUTHOR CONTRIBUTIONS

T.D. and W.-D.H. conceived the study. T.D., A.A.M., L.J.P., B.F., M.E.S., S.N., B.D.N., and S.Y.W. carried out experiments and interpreted data. R.F. and C.v.M. performed the cluster analysis, S.N. and M.H. performed the immunohistochemistry. C.M. supported the design of experiments. T.D. and W.-D.H wrote the manuscript.

ACKNOWLEDGMENTS

We thank A. Oxenius, R. Spörri, S. LeibundGut-Landmann, and M. Detmar for reagents; R. Spörri, S. LeibundGut-Landmann, F. Sparber, E. Steiner, J. Brasseit, M. Noti, A. Macpherson, M. Gomez de Aguero, D. Finke, A. Bärenwaldt, and M. Kopf for scientific discussion; J. Hehl, L. Dieterich, M. Barthel Scherrer, P. Peretti, D. Mbye, M. Kisielow, and A. Schütz for technical assistance; the RCHCI, the EPIC, the ScopeM, and the IMHS Flow Cytometry Core Facility for their excellent support. This work was supported by SNSF grants SNF 310030_132997, 310030_53074; CRSII3_136286, CRSII3_154414/1, SystemsX.ch, RTD 51RTP0_151029 (TargetInfectX), the Novartis Foundation (#15C181), the Helmut Horten Foundation, ETH Zürich (ETH-33 12-2) (to W.-D.H.) and a SRC fellowship 2012-262 (to M.E.S.).

Received: February 13, 2016
Revised: May 8, 2016
Accepted: June 14, 2016
Published: July 21, 2016

REFERENCES

Agnholt, J., Dahlerup, J.F., Buntzen, S., Tøttrup, A., Nielsen, S.L., and Lundorf, E. (2003). Response, relapse and mucosal immune regulation after infliximab treatment in fistulating Crohn's disease. Aliment. Pharmacol. Ther. *17*, 703–710.

Bain, C.C., and Mowat, A.M. (2011). Intestinal macrophages—specialised adaptation to a unique environment. Eur. J. Immunol. *41*, 2494–2498.

Barthel, M., Hapfelmeier, S., Quintanilla-Martínez, L., Kremer, M., Rohde, M., Hogardt, M., Pfeffer, K., Rüssmann, H., and Hardt, W.D. (2003). Pretreatment of mice with streptomycin provides a Salmonella enterica serovar Typhimurium colitis model that allows analysis of both pathogen and host. Infect. Immun. *71*, 2839–2858.

Bevins, C.L., and Salzman, N.H. (2011). Paneth cells, antimicrobial peptides and maintenance of intestinal homeostasis. Nat. Rev. Microbiol. *9*, 356–368.

Buckley, C.D., Gilroy, D.W., Serhan, C.N., Stockinger, B., and Tak, P.P. (2013). The resolution of inflammation. Nat. Rev. Immunol. *13*, 59–66.

Burrack, K.S., and Morrison, T.E. (2014). The role of myeloid cell activation and arginine metabolism in the pathogenesis of virus-induced diseases. Front. Immunol. *5*, 428.

Chassaing, B., Koren, O., Goodrich, J.K., Poole, A.C., Srinivasan, S., Ley, R.E., and Gewirtz, A.T. (2015). Dietary emulsifiers impact the mouse gut microbiota promoting colitis and metabolic syndrome. Nature *519*, 92–96.

Chiang, N., Fredman, G., Bäckhed, F., Oh, S.F., Vickery, T., Schmidt, B.A., and Serhan, C.N. (2012). Infection regulates pro-resolving mediators that lower antibiotic requirements. Nature *484*, 524–528.

Claudi, B., Spröte, P., Chirkova, A., Personnic, N., Zankl, J., Schürmann, N., Schmidt, A., and Bumann, D. (2014). Phenotypic variation of Salmonella in host tissues delays eradication by antimicrobial chemotherapy. Cell *158*, 722–733.

Diard, M., Sellin, M.E., Dolowschiak, T., Arnoldini, M., Ackermann, M., and Hardt, W.D. (2014). Antibiotic treatment selects for cooperative virulence of Salmonella typhimurium. Curr. Biol. *24*, 2000–2005.

Eberl, G. (2010). A new vision of immunity: homeostasis of the superorganism. Mucosal Immunol. *3*, 450–460.

Fonseca, D.M., Hand, T.W., Han, S.J., Gerner, M.Y., Glatman Zaretsky, A., Byrd, A.L., Harrison, O.J., Ortiz, A.M., Quinones, M., Trinchieri, G., et al. (2015). Microbiota-dependent sequelae of acute infection compromise tissue-specific immunity. Cell *163*, 354–366.

Germain, R.N. (2012). Maintaining system homeostasis: the third law of Newtonian immunology. Nat. Immunol. *13*, 902–906.

Godinez, I., Haneda, T., Raffatellu, M., George, M.D., Paixão, T.A., Rolán, H.G., Santos, R.L., Dandekar, S., Tsolis, R.M., and Bäumler, A.J. (2008). T cells help to amplify inflammatory responses induced by Salmonella enterica serotype Typhimurium in the intestinal mucosa. Infect. Immun. *76*, 2008–2017.

Gonzalez, M.D., Wilen, C.B., and Burnham, C.A. (2015). Markers of intestinal inflammation for the diagnosis of infectious gastroenteritis. Clin. Lab. Med. *35*, 333–344.

Gros, P., and Belkaid, Y. (2014). Editorial overview: Host pathogens. Curr. Opin. Immunol. *29*, iv–vi.

Hapfelmeier, S., Stecher, B., Barthel, M., Kremer, M., Müller, A.J., Heikenwalder, M., Stallmach, T., Hensel, M., Pfeffer, K., Akira, S., and Hardt, W.D. (2005). The Salmonella pathogenicity island (SPI)-2 and SPI-1 type III secretion systems allow Salmonella serovar typhimurium to trigger colitis via MyD88-dependent and MyD88-independent mechanisms. J. Immunol. *174*, 1675–1685.

Helaine, S., Cheverton, A.M., Watson, K.G., Faure, L.M., Matthews, S.A., and Holden, D.W. (2014). Internalization of Salmonella by macrophages induces formation of nonreplicating persisters. Science *343*, 204–208.

Hu, V.H., Holland, M.J., and Burton, M.J. (2013). Trachoma: protective and pathogenic ocular immune responses to Chlamydia trachomatis. PLoS Negl. Trop. Dis. *7*, e2020.

Janakiram, N.B., Mohammed, A., and Rao, C.V. (2011). Role of lipoxins, resolvins, and other bioactive lipids in colon and pancreatic cancer. Cancer Metastasis Rev. *30*, 507–523.

Jung, S., Aliberti, J., Graemmel, P., Sunshine, M.J., Kreutzberg, G.W., Sher, A., and Littman, D.R. (2000). Analysis of fractalkine receptor CX(3)CR1 function by targeted deletion and green fluorescent protein reporter gene insertion. Mol. Cell. Biol. *20*, 4106–4114.

Kaiser, P., Diard, M., Stecher, B., and Hardt, W.D. (2012). The streptomycin mouse model for Salmonella diarrhea: functional analysis of the microbiota, the pathogen's virulence factors, and the host's mucosal immune response. Immunol. Rev. *245*, 56–83.

Kaiser, P., Regoes, R.R., Dolowschiak, T., Wotzka, S.Y., Lengefeld, J., Slack, E., Grant, A.J., Ackermann, M., and Hardt, W.D. (2014). Cecum lymph node dendritic cells harbor slow-growing bacteria phenotypically tolerant to antibiotic treatment. PLoS Biol. *12*, e1001793.

Kaur, M., Bell, T., Salek-Ardakani, S., and Hussell, T. (2015). Macrophage adaptation in airway inflammatory resolution. Eur. Respir. Rev. *24*, 510–515.

Kirk, M.D., Pires, S.M., Black, R.E., Caipo, M., Crump, J.A., Devleesschauwer, B., Döpfer, D., Fazil, A., Fischer-Walker, C.L., Hald, T., et al. (2015). World Health Organization estimates of the global and regional disease burden of 22 foodborne bacterial, protozoal, and viral diseases, 2010: a data synthesis. PLoS Med. *12*, e1001921.

Koh, S.J., Lee, D.H., Lee, S.H., Park, Y.S., Hwang, J.H., Kim, J.W., Jeong, S.H., Kim, N., Im, J.P., Kim, J.S., et al. (2012). Incidence and risk factors of irritable bowel syndrome in community subjects with culture-proven bacterial gastroenteritis. Korean J. Gastroenterol. *60*, 13–18.

Levy, B.D., and Serhan, C.N. (2014). Resolution of acute inflammation in the lung. Annu. Rev. Physiol. *76*, 467–492.

Luo, C.L., Li, Q.Q., Chen, X.P., Zhang, X.M., Li, L.L., Li, B.X., Zhao, Z.Q., and Tao, L.Y. (2013). Lipoxin A4 attenuates brain damage and downregulates the production of pro-inflammatory cytokines and phosphorylated mitogen-activated protein kinases in a mouse model of traumatic brain injury. Brain Res. *1502*, 1–10.

Maltez, V.I., Tubbs, A.L., Cook, K.D., Aachoui, Y., Falcone, E.L., Holland, S.M., Whitmire, J.K., and Miao, E.A. (2015). Inflammasomes coordinate pyroptosis and natural killer cell cytotoxicity to clear infection by a ubiquitous environmental bacterium. Immunity *43*, 987–997.

GBD 2013 Mortality and Causes of Death Collaborators (2015). Global, regional, and national age-sex specific all-cause and cause-specific mortality for 240 causes of death, 1990-2013: a systematic analysis for the Global Burden of Disease Study 2013. Lancet *385*, 117–171.

Murray, P.J., and Wynn, T.A. (2011). Protective and pathogenic functions of macrophage subsets. Nat. Rev. Immunol. *11*, 723–737.

Murray, C.J., Barber, R.M., Foreman, K.J., Abbasoglu Ozgoren, A., Abd-Allah, F., Abera, S.F., Aboyans, V., Abraham, J.P., Abubakar, I., Abu-Raddad, L.J., et al.; GBD 2013 DALYs and HALE Collaborators (2015). Global, regional, and national disability-adjusted life years (DALYs) for 306 diseases and injuries and healthy life expectancy (HALE) for 188 countries, 1990-2013: quantifying the epidemiological transition. Lancet *386*, 2145–2191.

Onwuezobe, I.A., Oshun, P.O., and Odigwe, C.C. (2012). Antimicrobials for treating symptomatic non-typhoidal Salmonella infection. Cochrane Database Syst. Rev. *11*, CD001167.

Osborne, L.C., Monticelli, L.A., Nice, T.J., Sutherland, T.E., Siracusa, M.C., Hepworth, M.R., Tomov, V.T., Kobuley, D., Tran, S.V., Bittinger, K., et al. (2014). Coinfection. Virus-helminth coinfection reveals a microbiota-independent mechanism of immunomodulation. Science *345*, 578–582.

Saleh, M., and Elson, C.O. (2011). Experimental inflammatory bowel disease: insights into the host-microbiota dialog. Immunity *34*, 293–302.

Scallan, E., Hoekstra, R.M., Mahon, B.E., Jones, T.F., and Griffin, P.M. (2015). An assessment of the human health impact of seven leading foodborne pathogens in the United States using disability adjusted life years. Epidemiol. Infect. *143*, 2795–2804.

Schreiber, S., Rosenstiel, P., Hampe, J., Nikolaus, S., Groessner, B., Schottelius, A., Kühbacher, T., Hämling, J., Fölsch, U.R., and Seegert, D. (2002). Activation of signal transducer and activator of transcription (STAT) 1 in human chronic inflammatory bowel disease. Gut *51*, 379–385.

Schwille-Kiuntke, J., Unverdorben, A., Weimer, K., Schlarb, A.A., Gulewitsch, M.D., Ellert, U., and Enck, P. (2015). Bacterial infections in childhood: a risk factor for gastrointestinal and other diseases? United European Gastroenterol. J. *3*, 31–38.

Serhan, C.N. (2014). Pro-resolving lipid mediators are leads for resolution physiology. Nature *510*, 92–101.

Sirinavin, S., and Garner, P. (2000). Antibiotics for treating salmonella gut infections. Cochrane Database Syst. Rev. (2), CD001167.

Songhet, P., Barthel, M., Stecher, B., Müller, A.J., Kremer, M., Hansson, G.C., and Hardt, W.D. (2011). Stromal IFN-γR-signaling modulates goblet cell function during Salmonella Typhimurium infection. PLoS ONE *6*, e22459.

Sonnenberg, G.F., Fouser, L.A., and Artis, D. (2011). Border patrol: regulation of immunity, inflammation and tissue homeostasis at barrier surfaces by IL-22. Nat. Immunol. *12*, 383–390.

Stecher, B., Robbiani, R., Walker, A.W., Westendorf, A.M., Barthel, M., Kremer, M., Chaffron, S., Macpherson, A.J., Buer, J., Parkhill, J., et al. (2007). Salmonella enterica serovar typhimurium exploits inflammation to compete with the intestinal microbiota. PLoS Biol. *5*, 2177–2189.

Stelter, C., Käppeli, R., König, C., Krah, A., Hardt, W.D., Stecher, B., and Bumann, D. (2011). Salmonella-induced mucosal lectin RegIIIβ kills competing gut microbiota. PLoS ONE *6*, e20749.

Sylvester, F.A., Draghi, A., Menoret, A., Fernandez, M.L., Wang, Z., and Vella, A.T. (2014). Distinctive colonic mucosal cytokine signature in new-onset, untreated pediatric Crohn disease. J. Pediatr. Gastroenterol. Nutr. *59*, 553–561.

Tamoutounour, S., Henri, S., Lelouard, H., de Bovis, B., de Haar, C., van der Woude, C.J., Woltman, A.M., Reyal, Y., Bonnet, D., Sichien, D., et al. (2012). CD64 distinguishes macrophages from dendritic cells in the gut and reveals the Th1-inducing role of mesenteric lymph node macrophages during colitis. Eur. J. Immunol. *42*, 3150–3166.

Wirtz, S., Neufert, C., Weigmann, B., and Neurath, M.F. (2007). Chemically induced mouse models of intestinal inflammation. Nat. Protoc. *2*, 541–546.